Spatiotemporal Symmetries in the Disynaptic Canal-Neck Projection

Martin Golubitsky
Department of Mathematics
University of Houston
Houston TX 77204-3008, USA

LieJune Shiau
Department of Mathematics
University of Houston-Clear Lake
Houston TX 77058, USA

Ian Stewart
Mathematics Institute
University of Warwick
Coventry CV4 7AL, UK

March 2, 2007

Abstract

The vestibular system in almost all vertebrates, and in particular in humans, controls balance by employing a set of six semicircular canals, three in each inner ear, to detect angular accelerations of the head in three mutually orthogonal coordinate planes. Signals from the canals are transmitted to eight (groups of) neck motoneurons, which activate the eight corresponding muscle groups. These signals may be either excitatory or inhibitory, depending on the direction of acceleration. McCollum and Boyle have observed that in the cat the network of neurons concerned possesses octahedral symmetry, a structure that they deduce from the known innervation patterns (connections) from canals to muscles.

We re-derive the octahedral symmetry from mathematical features of the probable network architecture, and model the movement of the head in response to the activation patterns of the muscles concerned. We assume that connections between neck muscles can be modeled by a 'coupled cell network', a system of coupled ODEs whose variables correspond to the eight muscles, and that this network also has octahedral symmetry. The network and its symmetries imply that these ODEs must be equivariant under a suitable action of the octahedral group.

It is observed that muscle motoneurons form natural 'push-pull pairs' in which, for given movements of the head, one neuron produces an excitatory signal whereas the

other produces an inhibitory signal. By incorporating this feature into the mathematics in a natural way, we are led to a model in which the octahedral group acts by signed permutations on muscle motoneurons.

We show that with the appropriate group actions, there are six possible spatiotemporal patterns of time-periodic states that can arise by Hopf bifurcation from an equilibrium representing an immobile head. Here we use results of Ashwin and Podvigina. Counting conjugate states, whose physiological interpretations can have significantly different features, there are 15 patterns of periodic oscillation, not counting left-right reflections or time-reversals as being different. We interpret these patterns as motions of the head and note that all six types of pattern appear to correspond to natural head motions.

1 Introduction

The human vestibular system is a system of tubes that contain sensors for the sense of balance. There are two main components: the otolith organs, which sense linear acceleration of the head (translation), and the semicircular canals, which sense angular acceleration of the head (rotation). Each ear contains three semicircular canals (henceforth 'canals') arranged in three approximately mutually orthogonal planes. See Figure 1. A similar arrangement occurs in most vertebrates. We do not discuss the otolith system or other physiological features of the sense of balance.

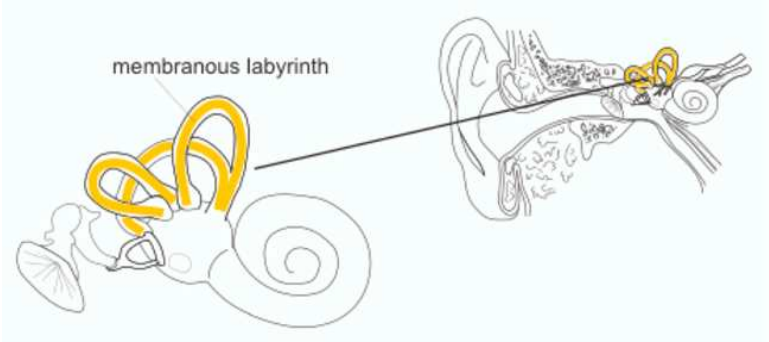

Figure 1: Structure and location of the semicircular canals (right ear). From Vilis [17].

In this paper we focus on two points. First, we rederive the symmetry group Γ of the network of neurons that conveys signals from the six canals to eight principal muscle groups that control the position of the neck. McCollum and Boyle [12] analyzed experimental work of Shinoda *et al.* [14, 15, 16] and Wilson and Maeda [18] to discover these symmetries. Our derivation makes transparent the fact that Γ is the 48 element symmetry group of the cube, which is called the *octahedral* group. This network of connections is known as the *canal-neck*

projection.

Second, we assume that the octahedral group Γ is also the symmetry group of the internal dynamics of the muscles and associated neural connections and we use these symmetries to discuss natural rhythmic head motions. We look only for small amplitude periodic head motions that can be sustained by the neck muscles alone. In particular, we assume that the sensory inputs from the canals are not relevant, except to prescribe the symmetries of the system. A similar approach has been applied previously to spatiotemporal patterns in animal locomotion, see Buono and Golubitsky [3], Collins and Stewart [4, 5], Golubitsky *et al.* [10, 11]. However, in those papers the patterns of locomotion were used to infer the symmetry of the network of neurons (central pattern generator) that produced them, whereas here we infer the patterns of movement from the known symmetries of the canal-neck projection.

Our approach is straightforward but not completely standard. The work of McCollum and Boyle [12] suggests a simplest network for the motoneurons of the eight muscle groups. Although we do not know (and perhaps cannot know) an accurate differential equations model for the (abstracted) muscle motoneurons, we can presume the form that such a model will take. We use the symmetries and the network structure to answer the question: What are the spatiotemporal symmetries of small amplitude periodic solutions that can be obtained by Hopf bifurcation from a group invariant equilibrium in this class of possible models? (These periodic solutions are the ones that can most naturally exist in models near a position where the head is held fixed and upright. A more general classification of the spatiotemporal symmetries of periodic solutions, whose amplitudes are not necessarily small, can be made using the H/K Theorem [3, 9]. However, we choose to begin our classification with the more restricted problem of small amplitude periodic solutions near an upright head.)

Using a caricature of the physical actions of the muscle groups, we observe that a group invariant equilibrium corresponds to one in which the head is held fixed. Using this caricature we can also interpret the form that the head motions will take based only on the spatiotemporal symmetries of the associated periodic solutions. In this sense our approach is model-independent; it does not depend on the particular system of ODEs. Our results provide a list, or menu, of the possible head motion types; specific models and specific parameters in the models choose from this menu and determine which solution types exist and which are stable. We do not discuss such model-dependent issues here.

In order to relate these spatiotemporal symmetries with characteristic head motions, we need to make assumptions about how the eight muscle groups move the head. For physiological and mathematical reasons we are led to classify the eight muscle groups into four opposing pairs. When both muscles in a pair are equally activated the head will not move. Indeed, to move the head, one muscle group must pull harder than the opposing one; we classify only those periodic states that satisfy this constraint.

To analyse the possible dynamics we employ the theory of dynamical systems with symmetry, which has implications for the dynamics of such a network. We restrict ourselves to classifying those types of head motions that can be described by small-amplitude periodic states near a group-invariant equilibrium. The mathematical tool for performing this classification is the Equivariant Hopf Bifurcation Theorem [8, 9]. In particular, we use the results of Ashwin and Podvigina [1] on Hopf bifurcation with octahedral symmetry.

This classification is 'model-independent' in the sense that it does not depend upon the detailed structure of the network of neurons concerned, or on the precise equations used to model neurons, provided the symmetry constraints are respected. Since all model equations in current use are primarily phenomenological, and the precise architecture of the muscle group network is unknown (even in the cat), model-independent results have a potential advantage: they depend only on the known symmetries of the network. Any specific choice of network architecture and model neuron dynamics (associated for example with particular vertebrate species) will generate a list of spatiotemporal patterns taken from the general classification, but with extra model-dependent restrictions on existence and stability. The model-independent features of the problem can also help to structure existence and stability calculations in specific models, see [9].

In order to create this menu and to make predictions about head motions, we must determine the appropriate 'phase space' variables upon which the group Γ acts, and also specify the appropriate group action. Our approach, as in the gaits work, is to use the network structure. We assume that each of the eight motoneurons (or more precisely, sets of motoneurons) are identified with variables in $\mathbf{R}^\ell$ so that the phase space of the muscle motoneurons is $Y = (\mathbf{R}^\ell)^8$. We also assume that the octahedral group acts on Y by permuting the coordinates, just as that group permutes the vertices of the cube. Next we assume that the differential equations that describe the time evolution of this coupled system of neck motoneurons have octahedral symmetry. Using this symmetry we can then classify the types of spatiotemporal symmetries that periodic states of such systems may have.

Specifically we find that there are six types of spatiotemporal symmetries for small amplitude periodic solutions that can bifurcate from a Γ-invariant equilibrium. Each of these symmetry types includes a reasonable pattern of periodic head motion. They are: shaking the head (saying 'no' in many cultures), which occurs in two different ways; nodding the head (saying 'yes' in those same cultures), a rotating wave in which the head rolls in an approximate horizontal circle, a combination of 'yes' and 'no' in which the head nods alternately to left and right, and a side to side motion with the head rotating to move the nose in the opposite direction (so that the nose always points at a fixed point in the distance).

Organization of the paper

In Section 2 we give a brief description of salient features of the physiology of the vestibular system, and rederive the octahedral symmetry of the canal-neck projection. We relate the associated network architecture to a graph drawn on a cube, and describe a simple caricature of the effects of the eight muscle groups. Section 3 describes the octahedral group in more detail and motivates the choice of action of this group on muscle space. This section also provides an explicit description of the permutation action of the octahedral group on muscle space, lists the relevant subgroups, and classifies the isotropy subgroups — basic data for the application of symmetric dynamics.

The Equivariant Hopf Theorem is described in Section 4, and a discussion of the irreducible representations of the octahedral group, the basic information needed for application of the Hopf theorem, is given. Proofs, which use character theory, are postponed to the Appendix. Section 5 presents a classification of the possible small-amplitude spatiotemporal symmetry patterns for time-periodic motions of the head, determined by the canal-neck projection. We find six distinct (conjugacy classes of) patterns, or 15 distinct patterns (not distinguishing time-reversals or left-right reflections in physical space). These patterns are interpreted as motions of the head in Section 6, assuming that the muscle groups act according to our caricature. We pay attention to distinctions arising from conjugate states.

We end with a short conclusions section.

2 Symmetries in the disynaptic canal-neck projection

In this section we rederive the symmetries in the disynaptic canal-neck projection discussed by McCollum and Boyle [12], stating the results in terms of a group of permutations acting on the associated network of neurons. In this aspect of the vestibular system there are six canals (three in each ear) that are connected to eight muscle groups in the neck.

The three canals located in each ear are called *horizontal* h, *anterior* a, and *posterior* p. We denote the six canals by lh, la, lp, rh, ra, rp, where l stands for *left* and r for *right*. Neurons associated to canal hairs have a base firing rate. These hairs are arranged so that fluid flow in one direction in the canal increases the firing rate and fluid flow in the opposite direction decreases that firing rate. Moreover, the canals are paired ({lh,rh}, {la,rp}, {lp,ra}), so that when one member of a pair transmits an elevated or excitated signal, then the other member of that pair transmits a reduced or inhibited one. These pairs are called *polarity pairs*.

The spatial arrangement of the canals is shown in Figure 2. There are three (approximately) mutually orthogonal planes. One of these planes is horizontal; the other two are vertical, at an angle of 45° to the plane of left-right symmetry of the head. Each polarity pair consists of two canals that are parallel to one of these planes: one canal in the left ear, one

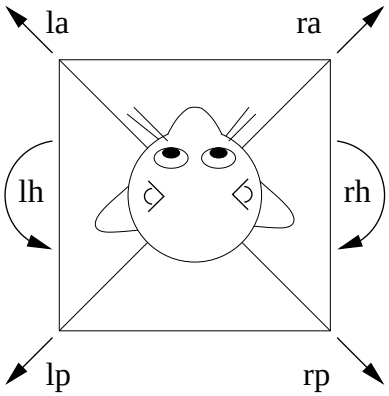

Figure 2: Location of the three planes relative to the head, and direction of rotational motion to which canals respond. Canals are drawn schematically near the ears.

in the right. These two canals are oriented in opposite directions in that plane and detect rotations (actually angular accelerations) of the head about an axis perpendicular to that plane. One member of the polarity pair detects acceleration in one orientation (clockwise or counterclockwise) and the other member detects the opposite orientation, as illustrated by the arrows in Figure 2. The four arrows at the corners represent rotations in the direction 'along the arrow and down'. For example, ra responds to motion in which the nose and right ear move forward to the left and down, while lp responds to motion in which the nose and right ear move backward to the right and up.

Connections from canals to muscles

Experiments show that each of the six canals can transmit signals to each of the eight muscle groups. The muscles also form four polarity pairs; if a canal is activated by the motion of the head, then it sends an excitatory signal to one member of each pair and an inhibitory signal to the other member. Physiological investigations (Wilson and Maeda [18], Shinoda *et al.* [14, 15, 16]) suggest that each muscle group is excited by a set of three mutually orthogonal canals (that is, one from each polarity pair) and inhibited by the complementary set of canals (the other members of the polarity pairs).

We describe the details of this arrangement, following McCollum and Boyle, who depict the list of signals transmitted to a given muscle group by an 'asterisk', Figure 3. Each asterisk has three solid lines (inhibitory connections) and three dotted lines (excitatory connections) and diametrically opposite lines have opposite polarity. There are eight possible arrangements of this type. Because the asterisks are drawn in two-dimensional projection, in a conventional orientation with lh between la and lp, there appear to be two kinds of asterisks: two alternating (with excitation and inhibition alternating) and six non-alternating (with

three contiguous excitatory canals). We will shortly see that under a suitable action of the octahedral group, all eight asterisks are equivalent.

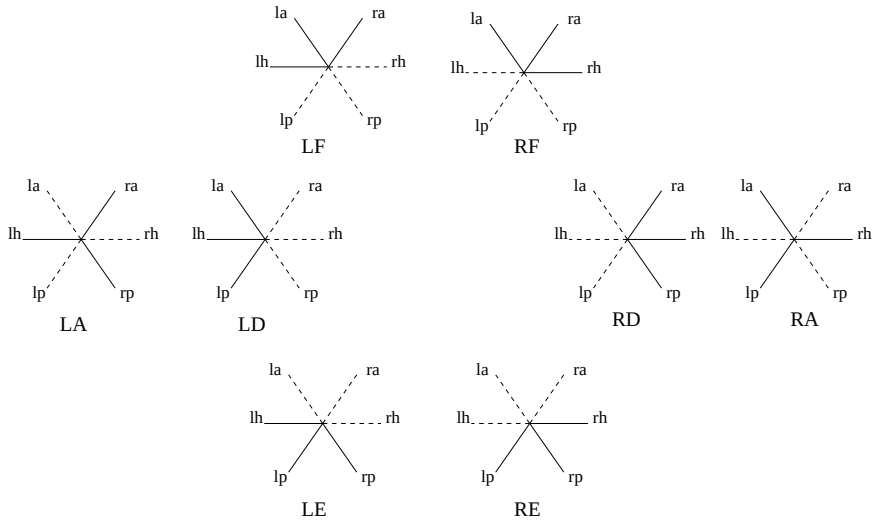

Figure 3: Innervation patterns corresponding to eight muscle groups. Dashed lines represent excitatory connections and solid lines inhibitory ones.

The eight neck muscles consist of two flexors in the front (LF, RF), two extensors in the back (LE, RE), and four side (shoulder) muscles. The side muscles are alternating (LA, RA) or directed (LD, RD). McCollum and Boyle [12] discuss the innervation patterns between canal neurons and muscle motoneurons—how the six canal neurons connect to the eight muscle motoneurons, and whether the connection occurs via an excitatory synapse or an inhibitory one. The pattern of connections to each muscle is specified by Figure 3. Each asterisk in Figure 3 is a list of the connections from all six canals to one muscle group, and the type of signal that is transmitted along each connection. Observe that the muscle groups also partition into four polarity pairs:

$$\{LA, RA\} \quad \{LF, RE\} \quad \{LE, RF\} \quad \{LD, RD\}.$$

If one muscle in a polarity pair has an excitatory connection from a canal, then the other muscle in that polarity pair has an inhibitory connection from that canal.

It is useful to display the same information in two other ways. McCollum and Boyle [12] consider only the *disynaptic pathway* from the six vestibular nerve afferents ('canal nerves') to the eight neck motoneurons (by way of the corresponding vestibulospinal neurons). They remark that almost always 'the motoneurons of each tested muscle responded to stimulation of all six canal nerves'. The responses were classified as either inhibitory or excitatory, as indicated by solid or dotted lines for the relevant arm of the asterisk. This description makes it clear that their Figure 4 (and our Figure 3) is a diagram determining these *connections*.

We make the connection pattern explicit. Figure 4 (left) shows connections to a given neck motoneuron, here LA. The associated asterisk is drawn and the six connections correspond to the six arms. Figure 4 (right) shows connections from a given vestibular nerve afferent, here lh. These connections correspond to the eight lh arms in the different asterisks, and connect to the corresponding neck motoneurons.

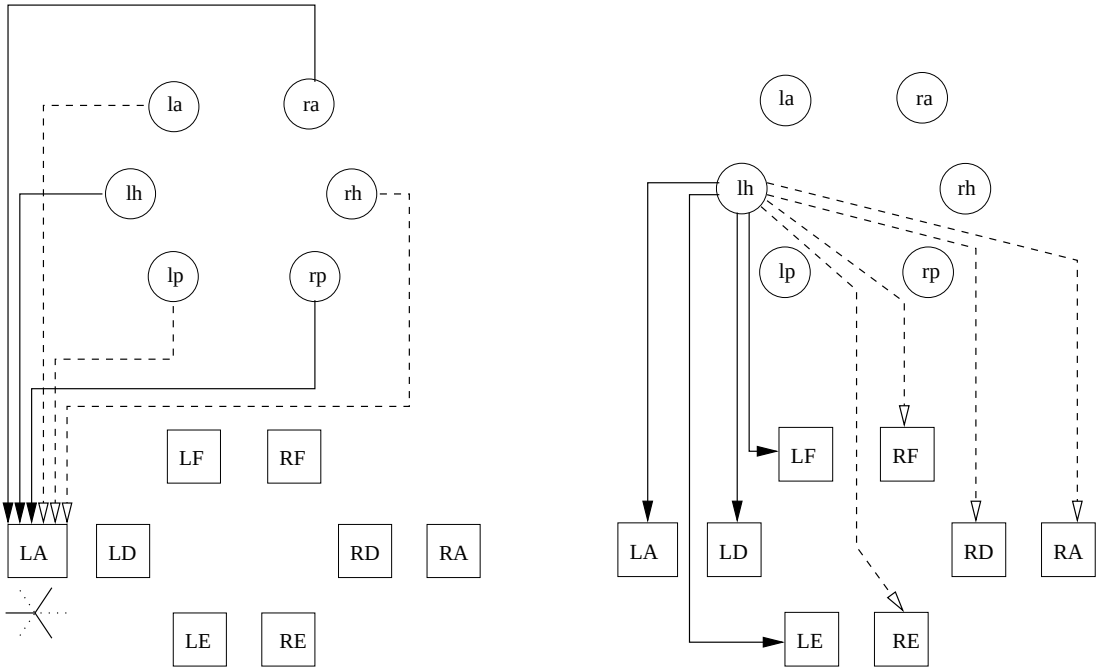

Figure 4: Schematic of connections from vestibular nerve afferent to neck motoneuron. Solid line shows inhibitory synapse, dotted line shows excitatory synapse. (Left) Connections to a given neck motoneuron, here LA. (Right) Connections from a given vestibular nerve afferent, here lh.

We do not attempt to draw the complete network since it would contain 48 lines, 24 solid and 24 dotted, and it would be too complicated to convey useful information. However, it is convenient to employ a geometric image in which the canals are identified with the six faces of a cube, and the muscles with the eight vertices. We will describe the network connectivity using the cube.

Octahedral symmetry of canals and muscles

The cube arises naturally from the results of McCollum and Boyle [12], identifying the symmetry group of the canal-neck projection as the 48-element octahedral group. To understand their observation, we identify the canals with faces of a cube, so that polarity pairs of canals

are identified with pairs of opposite faces. Up to symmetry there is only one way to make this identification.

To identify the muscles, we observe that every vertex of the cube is in the intersection of exactly three faces. We identify a given vertex with that muscle that has inhibitory connections from canals corresponding to the three faces adjacent to that vertex. For example there is a unique vertex that is in the intersection of the three faces corresponding to the left canals lh, lp, la (see Figure 5). We identify this vertex with the left direct muscle LD in Figure 3, since that muscle responds to inhibitory signals from the three left canals.

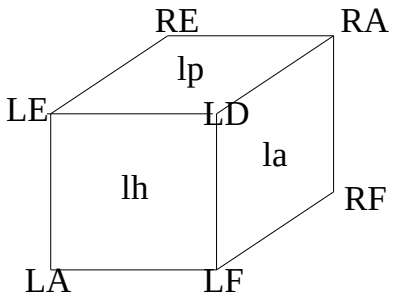

Figure 5: Identification of polarity pairs and muscle groups to the cube.

In Figure 6 we show the 24 inhibitory connections on the cube diagram. The complementary set of connections from canal neurons to muscle motoneurons consist of excitatory connections, but is omitted for clarity. The octahedral symmetry of the network is apparent in this figure. The elements of the octahedral group act on the full network by permuting canals, permuting muscles, and permuting the corresponding connections.

Muscle group action: a caricature

What effect do the eight muscle groups have on the head? For purposes of interpretation, we adopt a caricature of the anatomy of the muscle groups, illustrated in Figure 7. Here we assume that the principal effect of a muscle group being activated is to pull the head in the indicated direction. Six muscle groups LF, LD, LE, RF, RD, RE effectively form a 'hexagon' and their effect is to tilt the head in various directions. The other two, LA and RA, rotate the head about the vertical axis (as sensed by the horizontal canals lh, rh). There is some redundancy here: the hexagon includes three pairs of muscle groups but the three associated directions are linearly dependent. However, the use of six muscles makes the head position more stable, so there may be physiological reasons for this redundancy. McCollum and Boyle [12] call this hexagon the 'central dial'. This caricature exhibits the four pairs of opposing muscles (LD, RD), (LE, RF), (LF, RE), (LA, RA), which are just the four polarity pairs.

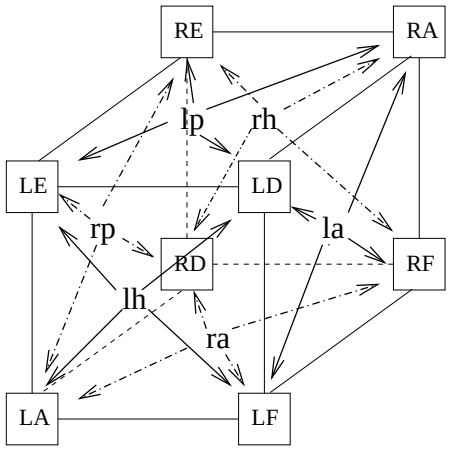

Figure 6: Schematic of inhibitory connections from canals to muscles drawn on the cube. Solid lines show connections on 'visible' faces, dot/dashed lines show connections on 'hidden' faces. Canals are at centers of faces, muscles at vertices. Connections run to each vertex from the three adjacent faces. The octahedral symmetry of the network is obvious geometrically.

We stress that this picture of the anatomy is a caricature. At this stage we make no attempt to formulate a more realistic model of the physiology and the mechanics of head movement. However, further detail of this kind could be developed without changing the classification of possible symmetry types of time-periodic motion. What would change would be the fine detail of the corresponding head motions, and the precise manner in which each muscle group contributes to that motion.

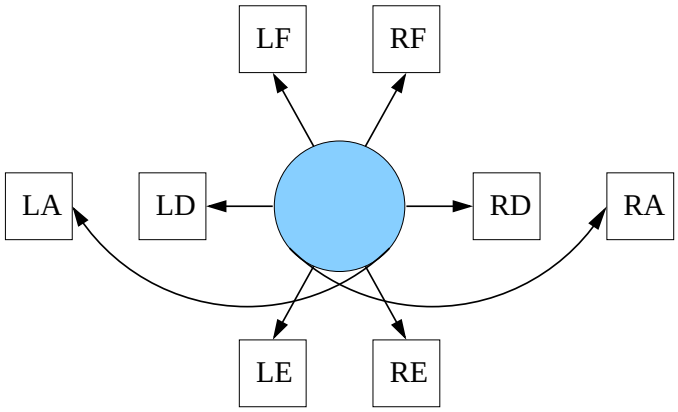

Figure 7: Caricature of effect of activation of muscle groups.

3 The octahedral group and its actions

We now discuss mathematical features of the octahedral group, and various actions of that group that occur in this analysis. In particular, we introduce variables that model the state of the eight muscle groups, and discuss how the octahedral groups acts on those variables.

The geometry of Figure 6, together with the corresponding figure for excitatory connections (which has the same symmetry), shows that the network of neurons forming the canal-neck projection has octahedral symmetry, where now the octahedral group acts by permuting the 8 muscle groups, the 6 canal neurons, and the connections between them. These permutation actions are distinct from, but induced naturally by, the 'standard' action as isometries of $\mathbf{R}^3$ that preserve the cube.

Suppose we fix the cube so that it is centered at the origin. Then the symmetries of the cube have the form R or $-R$ where R is a rotation. It follows that the octahedral group is the direct sum of the group $\mathbb{O}$ of rotation symmetries of the cube and the two-element group $\mathbf{Z}_2^c$ generated by the inversion $-I$. That is, the octahedral group is $\mathbb{O} \oplus \mathbf{Z}_2^c$. The '$c$' in the notation $\mathbf{Z}_2^c$ indicates that this group is the center of the octahedral group.

We are modeling the canal-neck projection by a network of interconnecting neurons, following Figures 4 and 6. This network has symmetry group $\mathbb{O} \oplus \mathbf{Z}_2^c$, which acts on the network by permuting the set of cells and the set of arrows. This permutation action preserves the type of the cell (canal neuron, shown as a circle, or muscle motoneuron, shown as a square), and it preserves the type of arrow (inhibitory or excitatory).

Phase space for muscles

This permutation action can be transferred to the dynamical variables representing the states of the cells; that is, the phase space of the network. We now describe the effect of this action on the 8 muscle cells. In order to do this we order the eight vertices as in (3.1). The ordering is shown on the cube in Figure 8.

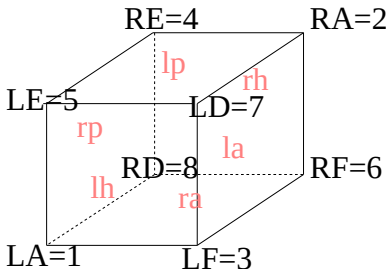

Figure 8: Ordering of vertices.

The simplest model for a state of the eight muscle motoneurons is a point in $\mathbf{R}^8$, with

coordinates

$$(y_{\mathrm{LA}}, y_{\mathrm{RA}}, y_{\mathrm{LF}}, y_{\mathrm{RE}}, y_{\mathrm{LE}}, y_{\mathrm{RF}}, y_{\mathrm{LD}}, y_{\mathrm{RD}}) \tag{3.1}$$

Each element of $\mathbb{O} \oplus \mathbf{Z}_2^c$ permutes the eight subscripts LA, RA, LF, RE, LE, RF, LD, RD according to the associated transformation of the vertices of the cube in Figure 8. The overall phase space for any system of ODEs representing the dynamics of the network, consistent with the $\mathbb{O} \oplus \mathbf{Z}_2^c$ symmetry, is therefore equivariant for the permutation action of $\mathbb{O} \oplus \mathbf{Z}_2^c$ on the space $\mathbf{R}^8$.

Our goal is to determine the spatiotemporal symmetries of small amplitude periodic solutions that can be obtained from a synchronous equilibrium by Hopf bifurcation. An important step in this analysis is the computation of the irreducible representations of the symmetry group $\mathbb{O} \oplus \mathbf{Z}_2^c$ on $(\mathbf{R}^\ell)^8$. However, up to isomorphism the answer for general ℓ is identical to the case when $\ell = 1$, for the following reason. Because the group acts by permutations (see the next subsection), the action on $(\mathbf{R}^\ell)^8$ consists of ℓ isomorphic copies of the action on $\mathbf{R}^8$. So the isomorphism types of the irreducible components are the same for all ℓ. However, their multiplicities depend on ℓ. We return to this point in Section 4.

The action of $\mathbb{O} \oplus \mathbf{Z}_2^c$ is determined by that of $\mathbb{O}$ and that of $\mathbf{Z}_2^c$. A crucial feature of the 'cube' structure is that the action of $-I$ preserves polarity pairs {LA,RA}, {LF, RE}, {LE, RF}, and {LD, RD}, because they label pairs of opposite vertices. Their entries are interchanged by $-I$. That is, $-I$ acts as the permutation

$$(1\ 2)(3\ 4)(5\ 6)(7\ 8)$$

Permutation action of $\mathbb{O}$ on muscle space

It remains to analyse the action of $\mathbb{O}$. We begin the discussion of the action of $\mathbb{O}$ on $\mathbf{R}^8$ by describing how it acts by rotations on $\mathbf{R}^3$ in the 'cube' picture. There are three types of rotation: rotations about axes connecting centers of opposite faces, rotations about axes connecting midpoints of opposite edges, and rotations about axes containing opposite vertices. There are 9 rotations corresponding to faces, since there are three pairs of faces and each pair determines three nonidentity rotations. There are 6 rotations corresponding to edges, since there are six pairs of edges and each pair determines just one nonidentity rotation. There are 8 rotations corresponding to vertices, since there are four pairs of vertices and each pair determines two nonidentity rotations.

Denote by V_j the clockwise rotation of 120° about the axis through vertex j for $j = 1, \ldots, 8$ ('clockwise' when viewed with vertex j nearest to the eye). Note that $V_1^2 = V_2$, $V_3^2 = V_4$, $V_5^2 = V_6$, $V_1^7 = V_8$. Denote by F_j the clockwise rotation of 90° about the axis perpendicular to face j for $j = 1, \ldots, 6$. Note that $F_1^3 = F_2$, $F_3^3 = F_4$, $F_5^3 = F_6$. Let $A_i = F_{2i-1}^2$ for $i = 1, 2, 3$. Then the F_j and the A_i are the nine rotations about axes connecting midpoints of opposite faces. Finally, note that each edge is uniquely the intersection of two

I	I
V_1	(3 8 5)(4 7 6)
V_2	(3 5 8)(4 6 7)
V_3	(1 7 6)(2 8 5)
V_4	(1 6 7)(2 5 8)
V_5	(1 4 7)(2 3 8)
V_6	(1 7 4)(2 8 3)
V_7	(1 4 6)(2 3 5)
V_8	(1 6 4)(2 5 3)
A_1	(1 7)(2 8)(3 5)(4 6)
A_2	(1 4)(2 3)(5 8)(6 7)
A_3	(1 6)(2 5)(3 8)(4 7)

F_1	(1 5 7 3)(2 6 8 4)
F_2	(1 3 7 5)(2 4 8 6)
F_3	(1 5 4 8)(2 6 3 7)
F_4	(1 8 4 5)(2 7 3 6)
F_5	(1 8 6 3)(2 7 5 4)
F_6	(1 3 6 8)(2 4 5 7)
E_{13}	(1 2)(3 7)(4 8)(5 6)
E_{14}	(1 5)(2 6)(3 4)(7 8)
E_{15}	(1 2)(3 4)(5 7)(6 8)
E_{16}	(1 3)(2 4)(5 6)(7 8)
E_{35}	(1 8)(2 7)(3 4)(5 6)
E_{45}	(1 2)(3 6)(4 5)(7 8)

Table 1: Permutation actions on $\mathbf{R}^8$ of rotations in $\mathbb{O}$.

subgroup	order	generators	normalizer
$\mathbf{Z}_2^A$	2	A_3	$\mathbf{D}_4$
$\mathbf{Z}_2^E$	2	E_{16}	$\mathbf{D}_2^E$
$\mathbf{Z}_3$	3	V_1	$\mathbf{S}_3$
$\mathbf{D}_2^A$	4	A_1, A_3	$\mathbb{O}$
$\mathbf{D}_2^E$	4	E_{15}, E_{16}	$\mathbf{D}_4$

subgroup	order	generators	normalizer
$\mathbf{Z}_4$	4	F_3	$\mathbf{D}_4$
$\mathbf{S}_3$	6	E_{15}, V_1	$\mathbf{S}_3$
$\mathbf{D}_4$	8	A_3, F_3	$\mathbf{D}_4$
$\mathbb{T}$	12	A_3, V_4	$\mathbb{O}$
$\mathbb{O}$	24	V_4, F_5	$\mathbb{O}$

Table 2: The 10 nonidentity subgroups of $\mathbb{O}$ up to conjugacy, with generators.

faces. Denote by E_{ij} the rotation by 180° about the edge in the intersection of faces i and j, where $i < j$. There are six possibilities.

In Table 1 we list the 24 rotations and their permutation actions on $\mathbf{R}^8$. The entries can be read off easily from Figure 8.

Subgroups of $\mathbb{O}$

We use the following notation for groups: $\mathbf{Z}_k$ is the cyclic group of order k, $\mathbf{D}_k$ is the dihedral group of order k, $\mathbf{S}_k$ is the symmetric group of degree k, and $\mathbb{T}$ is the tetrahedral group. This is the unique subgroup of $\mathbb{O}$ that has order 12, and it fixes a tetrahedron inscribed in the cube. Table 2 lists the 11 conjugacy classes of subgroups of $\mathbb{O}$. This calculation was done using the algebra program GAP.

4 Types of Hopf bifurcation

Hopf bifurcation is the tool for finding small-amplitude periodic states near an equilibrium. Equivariant Hopf theory [8, 9] states that there is a different type of Hopf bifurcation from a group-invariant equilibrium for each irreducible representation of the group. The Equivariant Hopf Theorem helps classify the types of spatiotemporal symmetries of periodic states that emanate from a given Hopf bifurcation. We apply this theory in the case of $\mathbb{O} \oplus \mathbf{Z}_2^c$ acting on muscle space $(\mathbf{R}^\ell)^8$ where the equilibrium is $\mathbb{O} \oplus \mathbf{Z}_2^c$-invariant. At such an equilibrium opposing muscles act with equal strength, so that the head is fixed and upright.

As noted previously, the types of irreducible representation of $\mathbb{O} \oplus \mathbf{Z}_2^c$ acting on $(\mathbf{R}^\ell)^8$ are identical with those of $\mathbb{O} \oplus \mathbf{Z}_2^c$ acting on $\mathbf{R}^8$. So the first step is to find the irreducible representations of $\mathbb{O} \oplus \mathbf{Z}_2^c$ acting on $\mathbf{R}^8$. We will show that there are four different irreducible representations, only two of which can lead to periodic states corresponding to nontrivial head motions. One of the associated Hopf bifurcations is simple to analyze, and the other was analyzed previously by Ashwin and Podvigina [1].

Decomposition of $\mathbf{R}^8$ into 'push-pull' and 'pull-pull' subspaces

The irreducible representations are intimately associated with the action of the inversion $-I$, which plays a key role because it swaps the members of each pair of opposing muscle motoneurons.

We can decompose $\mathbf{R}^8 = Y^+ \oplus Y^-$ into two 4-dimensional $\mathbb{O} \oplus \mathbf{Z}_2^c$-invariant subspaces, so that $-I$ acts trivially on one subspace and changes sign on the other. To do so, define

$$Y^\pm = \{y \in \mathbf{R}^8 : y_{\mathrm{LA}} = \pm y_{\mathrm{RA}}, y_{\mathrm{LF}} = \pm y_{\mathrm{RE}}, y_{\mathrm{LE}} = \pm y_{\mathrm{RF}}, y_{\mathrm{LD}} = \pm y_{\mathrm{RD}}\}$$

Note that the coordinates corresponding to opposing muscle pairs in Y^+ are equal and the coordinates corresponding to opposing muscle pairs in Y^- are equal in magnitude but opposite in sign.

As noted previously, three polarity pairs of muscles (the central dial) pull the head in opposite directions, and the muscles of the fourth pair (the alternating muscles) twist the head in opposite directions. In states in Y^+ polarity pairs of muscles act as 'pull-pull' pairs, whereas in states in Y^- these polarity pairs act as 'push-pull' pairs. In fact, all muscles must be under tension; thus 'push-pull' pairs really operate with one muscle group pulling harder than usual while the other pulls less hard. Phenomenologically, we can identify the difference between the tensions of two muscles in a polarity pair with the deviation of the tension (of either muscle, subject to sign) from the rest tension in which the head remains upright.

Next we observe that Hopf bifurcation corresponding to an irreducible representation in Y^+ can only lead to periodic states in which the head is immobile. The reason is simple:

$Y^+ = \mathrm{Fix}(-I)$, which is flow-invariant. Thus, in the nonlinear theory, any periodic state emanating from such a bifurcation must itself be fixed by $-I$; consequently, the opposing muscles in each polarity pair are always pulling with the same strength, creating a net motion of zero. As well as being inefficient, this space of motions has no visible effect on the head. In contrast, on the space Y^-, opposing pairs of muscles cooperate to move the head in exactly the same manner, so the muscle actions reinforce each other.

In fact, neither subspace Y^+ and Y^- is irreducible; each subspace decomposes into a 1-dimensional and a 3-dimensional irreducible representation. The previous remark implies that we need focus only on the subspace $Y^- \cong \mathbf{R}^4$.

Decomposition of Y^- into irreducible subspaces

As we have seen, the inversion $-I$ interchanges the muscles in each polarity pair and the states in Y^- are ones of the form

$$(y_{\mathrm{LA}}, -y_{\mathrm{LA}}, y_{\mathrm{LF}}, -y_{\mathrm{LF}}, y_{\mathrm{LE}}, -y_{\mathrm{LE}}, y_{\mathrm{LD}}, -y_{\mathrm{LD}}) \tag{4.1}$$

that is, we can parametrize Y^- by the strengths of the four left muscle groups, which correspond to the muscle groups numbered $1, 3, 5, 7$. Thus we can rewrite (4.1) as

$$(y_1, -y_1, y_3, -y_3, y_5, -y_5, y_7, -y_7)$$

which we parametrize by (y_1, y_3, y_5, y_7).

On Y^- the action of $\mathbb{O} \oplus \mathbf{Z}_2^c$ can now be written using signed permutations, since this action preserves polarity pairs and introduces a minus sign when members of a polarity pair are swapped. In particular, we can identify the action of $-I$ on Y^- with the signed permutation $(-y_1, -y_3, -y_5, -y_7)$; that is, $-I$ acts by multiplication by -1 on Y^-, as expected. The signed permutation action of $\mathbb{O}$ on Y^- is given in Table 3.

The subspace Y^- contains the 1-dimensional (hence irreducible) subspace

$$Y_0^- = \mathbf{R}\{(1, -1, -1, 1, -1, 1, 1, -1)\}$$

upon which the elements A_3 and V_4, the generators of the tetrahedral group, act trivially. In addition, $(\mathbb{O} \setminus \mathbb{T}, -I)$ acts trivially, since both $\mathbb{O} \setminus \mathbb{T}$ and $-I$ act as multiplication by -1.

Let Y_1^- be the 3-dimensional invariant complement of Y_0^- in Y^-; so $Y^- = Y_0^- \oplus Y_1^-$. It can be shown that Y_1^- is irreducible, and the action of $\mathbb{O}$ on Y_1^- is isomorphic to the standard action of the cube on $\mathbf{R}^3$. We do this using character theory in the Appendix.

Recall that for modeling purposes we assume that the muscle state space Y^- consists of ℓ variables for each polarity pair of muscles. Thus $Y^- \cong (\mathbf{R}^\ell)^4$. As noted previously the minimal phase space for any of our models occurs when $\ell = 1$. Although the analysis of possible spatiotemporal patterns reduces to the case $\ell = 1$, when we come to consider Hopf

γ	Action on γ on Y^-
I	$(\ y_1,\ y_3,\ y_5,\ y_7)$
V_1	$(\ y_1,\ y_5, -y_7, -y_3)$
V_2	$(\ y_1, -y_7,\ y_3, -y_5)$
V_3	$(-y_5,\ y_3, -y_7,\ y_1)$
V_4	$(\ y_7,\ y_3, -y_1, -y_5)$
V_5	$(\ y_7, -y_1,\ y_5, -y_3)$
V_6	$(-y_3, -y_7,\ y_5,\ y_1)$
V_7	$(-y_5, -y_1,\ y_3,\ y_7)$
V_8	$(-y_3,\ y_5, -y_1,\ y_7)$
A_1	$(\ y_7,\ y_5,\ y_3,\ y_1)$
A_2	$(-y_3, -y_1, -y_7, -y_5)$
A_3	$(-y_5, -y_7, -y_1, -y_3)$

γ	Action on γ on Y^-
F_1	$(\ y_3,\ y_7,\ y_1,\ y_5)$
F_2	$(\ y_5,\ y_1,\ y_7,\ y_3)$
F_3	$(-y_7, -y_5,\ y_1,\ y_3)$
F_4	$(\ y_5,\ y_7, -y_3, -y_1)$
F_5	$(\ y_3, -y_5,\ y_7, -y_1)$
F_6	$(-y_7,\ y_1, -y_3,\ y_5)$
E_{13}	$(-y_1,\ y_7, -y_5,\ y_3)$
E_{14}	$(\ y_5, -y_3,\ y_1, -y_7)$
E_{15}	$(-y_1, -y_3,\ y_7,\ y_5)$
E_{16}	$(\ y_3,\ y_1, -y_5, -y_7)$
E_{35}	$(-y_7, -y_3, -y_5, -y_1)$
E_{45}	$(-y_1, -y_5, -y_3, -y_7)$

Table 3: Action of elements in $\mathbb{O}$ on muscle 'push-pull' polarity pair space Y^-.

bifurcation, it turns out that we must require $\ell \geq 2$. (Reason: equivariant Hopf bifurcation requires certain representations to appear twice, namely, the absolutely irreducible ones, and that multiplicity occurs only when $\ell \geq 2$. See [8, 9].) Since all neurons, and in particular muscle motoneurons, have high-dimensional internal dynamics, this condition poses no difficulties.

5 Symmetry types of periodic state

At a Γ-invariant equilibrium for a Γ-equivariant system of ODEs, the Equivariant Hopf Theorem [8, 9] states (under several genericity hypotheses) that there exists a branch of small-amplitude periodic states corresponding to every $\mathbf{C}$-axial subgroup of $\Gamma \times \mathbf{S}^1$ acting on the center subspace at that equilibrium. Moreover these periodic states have spatio-temporal symmetries given by the $\mathbf{C}$-axial subgroup. A subgroup of $\Gamma \times \mathbf{S}^1$ is $\mathbf{C}$-*axial* if it is an isotropy subgroup and its fixed-point subspace, within the eigenspace corresponding to the purely imaginary eigenvalues, has dimension 2.

A complete discussion of equivariant Hopf theory is beyond the scope of this paper; details can be found in [8, 9]. To simplify the remarks we make here, we assume that all periodic solutions have period 1. Then $\mathbf{S}^1$, the group of phase shift symmetries, is parameterized from 0 to 1. We now recall two general points from Hopf theory. First, the phase shift by $\frac{1}{2}$ acts as multiplication by -1 on the center subspace. Second, the kernel of the action of $\Gamma \times \mathbf{S}^1$ on the center subspace is contained in every $\mathbf{C}$-axial subgroup.

In the case at hand, we saw that $-I$ acts as multiplication by -1 on Y^-. Thus the element $(-I, \frac{1}{2})$ in $\mathbf{Z}_2^c \times \mathbf{S}^1$ acts trivially in any Hopf bifurcation with center subspace in Y^-. It follows that every periodic state emanating from such a bifurcation has the property that interchanging polarity pairs is the same as making a half period phase shift. That is,

$$\begin{array}{ll} y_2(t+\frac{1}{2}) = y_1(t) & y_4(t+\frac{1}{2}) = y_3(t) \\ y_6(t+\frac{1}{2}) = y_5(t) & y_8(t+\frac{1}{2}) = y_7(t) \end{array} \tag{5.1}$$

Dividing by the subgroup $\mathbf{Z}_2(-I, \frac{1}{2})$ leads to the standard action of $\mathbb{O} \times \mathbf{S}^1$ on the center subspace. To see this, consider the epimorphism $\varphi : (\mathbb{O} \oplus \mathbf{Z}_2^c) \times \mathbf{S}^1 \to \mathbb{O} \times \mathbf{S}^1$ defined by

$$\varphi(\gamma, I, \theta) = (\gamma, \theta) \quad \text{and} \quad \varphi(\gamma, -I, \theta) = (\gamma, \theta + \tfrac{1}{2})$$

The kernel of φ is $\mathbf{Z}_2(-I, \frac{1}{2})$ and the quotient group is $\mathbb{O} \times \mathbf{S}^1$ with its standard action on Y^-, since $\varphi(\gamma, I, \theta) = (\gamma, \theta)$. It follows that to classify the relevant types of periodic solutions, we need only analyze those periodic solutions that occur in Hopf bifurcations associated to $\mathbb{O}$ acting on Y^- and then add in the constraints (5.1), if needed.

Using the decomposition of phase space into Y^+ and Y^- components, we can write any periodic state in the form $y(t) = y^+(t) + y^-(t)$. When, we come to interpret the motions associated with the periodic states, factoring out the Y^+ component will not change these motions in any important manner since, as discussed previously, $y^+(t)$ by itself leaves the head immobile. Moreover, near these Hopf bifurcations the Y^+ components will be small compared to the Y^- components. More precisely, suppose that a Hopf bifurcation supported in Y^- leads to a periodic state of amplitude ε. Then the theory implies that generically $y^-(t)$ will be of order ε, while $y^+(t)$ will be of order ε^2. Finally, coupling (5.1) with the definitions of Y^- and Y^+ leads to the conclusion that $y^+(t)$ oscillates with twice the frequency of $y^-(t)$ and that

$$\begin{array}{ll} y_1^-(t+\frac{1}{2}) = -y_1^-(t) & y_3^-(t+\frac{1}{2}) = -y_3^-(t) \\ y_5^-(t+\frac{1}{2}) = -y_5^-(t) & y_7^-(t+\frac{1}{2}) = -y_7^-(t) \end{array} \tag{5.2}$$

In short, when discussing small-amplitude periodic solutions of the nonlinear ODEs on muscle phase space, the system can effectively be reduced to an $\mathbb{O}$-equivariant system of ODEs on the reduced phase space Y^- whose periodic solutions also satisfy (5.2). It is this reduced system that we study for the remainder of this paper.

Spatiotemporal symmetries defined by H and K

In Γ-equivariant systems we can associate two subgroups H and K of Γ to each periodic state $y(t)$. Elements of the subgroup K fix the periodic trajectory pointwise, whereas elements of the subgroup H fix the periodic trajectory setwise. Uniqueness of solutions with a given initial condition implies that each element of H couples with a phase shift to fix the periodic state.

When $\ell \geq 2$, periodic states can have spatiotemporal symmetry group pairs (H, K) only if H/K is cyclic and K is an isotropy subgroup [9]. We describe the symmetries associated to periodic states obtained by Hopf bifurcation in terms of these (H, K) pairs.

Hopf bifurcation in Y^-

Next we classify the types of periodic state that can arise as a small-amplitude motion near the steady state (in which there is no head motion). Such states can be found using the Equivariant Hopf Theorem [8, 9]. This theorem states that there is a possible Hopf bifurcation corresponding to each irreducible representation of $\mathbb{O}$ acting on phase space. Now, the decomposition of Y^- into irreducibles can be viewed as a decomposition $\mathbf{R}^4 = W_0 \oplus W_1$ where

$$W_0 = \mathbf{R}\{(1,-1,-1,1)\} \quad \text{and} \quad W_1 = \mathbf{R}\{(1,1,1,1),(1,1,-1,-1),(1,-1,1,-1)\}.$$

Here W_0 corresponds to Y_0^- and W_1 corresponds to Y_1^-. Both are irreducible. The kernel of the action of $\mathbb{O}$ on W_0 is $\mathbb{T}$; the representation on W_1 is the standard three-dimensional irreducible representation, in which $\mathbb{O}$ acts as isometries that preserve the cube.

Hopf bifurcation via W_0 leads to periodic states with $H = \mathbb{O}$ and $K = \mathbb{T}$. Ashwin and Podvigina [1] classify the periodic states that arise from the standard irreducible representation of $\mathbb{O}$. This is the most difficult case for Hopf bifurcation. There are five types of periodic state, whose (H, K) pairs are $(\mathbf{D}_4, \mathbf{Z}_4)$, $(\mathbf{D}_2^E, \mathbf{Z}_2^E)$, $(\mathbf{Z}_4, \mathbf{1})$, $(\mathbf{S}_3, \mathbf{Z}_3)$ and $(\mathbf{Z}_3, \mathbf{1})$. Table 4 lists these pairs, together with associated information.

We sketch the derivation of the 'muscle oscillation' column of this table. Consider the pair $(H, K) = (\mathbb{O}, \mathbb{T})$ in the first row. Here $\mathbb{T}$ fixes the state of each muscle group at each time. By Table 2, the group $\mathbb{T}$ is generated by A_3 and V_4. Therefore, by Table 3, any state $y(t)$ with the symmetry pair $(\mathbb{O}, \mathbb{T})$ must satisfy

$$y_1(t) \equiv -y_5(t) \qquad y_3(t) \equiv -y_7(t) \qquad y_1(t) \equiv y_7(t)$$

so that

$$y(t) = (u(t), -u(t), -u(t), u(t))$$

for a time-periodic function u. The quotient H/K is isomorphic to $\mathbf{Z}_2$, and is generated (modulo K) by the element $(F_5, \frac{1}{2}) \in \mathbb{O} \times \mathbf{S}^1$. This imposes the same condition $u(t + \frac{1}{2}) = -u(t)$ that was previously noted using the symmetry $(-I, \frac{1}{2})$.

For a more complicated example, consider the pair $(H, K) = (\mathbf{Z}_3, \mathbf{1})$. Since K is trivial, no components of $y(t)$ are forced to be synchronous. The subgroup $\mathbf{Z}_3$ is generated by V_1, whose action on $\mathbf{R}^4$ fixes y_1 and cycles $(y_3, y_5, -y_7)$. The only possible pattern of phase shifts here is $(0, \frac{1}{3}\delta, \frac{2}{3}\delta)$, where $\delta = \pm 1$. So

$$((y_3(t), y_5(t), y_7(t)) = (u(t), u(t + \tfrac{1}{3}\delta), -u(t + \tfrac{2}{3}\delta)),$$

Type	H generators	K generators	Muscle oscillation	#
$(\mathbb{O}, \mathbb{T})$	V_4, F_5	V_4, A_3	$(u(t), -u(t), -u(t), u(t))$	1
$(\mathbf{S}_3, \mathbf{Z}_3)$	V_1, E_{15}	V_1	$(u(t), z(t), z(t), -z(t))$	2
	V_3, E_{14}	V_3	$(z(t), u(t), -z(t), z(t))$	3
	V_5, E_{16}	V_5	$(z(t), -z(t), u(t), z(t))$	
	V_7, E_{45}	V_7	$(-z(t), z(t), z(t), u(t))$	4
$(\mathbf{D}_2^E, \mathbf{Z}_2^E)$	E_{16}, E_{15}	E_{16}	$(u(t), u(t), 0, 0)$	5
	E_{14}, E_{13}	E_{14}	$(u(t), 0, u(t), 0)$	
	E_{45}, E_{35}	E_{45}	$(0, u(t), -u(t), 0)$	6
	E_{13}, E_{14}	E_{13}	$(0, u(t), 0, u(t))$	7
	E_{15}, E_{16}	E_{15}	$(0, 0, u(t), u(t))$	
	E_{35}, E_{45}	E_{35}	$(u(t), 0, 0, -u(t))$	8
$(\mathbf{Z}_4, \mathbf{1})$	F_1	I	$(u(t), u(t+\frac{1}{4}\delta), u(t+\frac{3}{4}\delta), u(t+\frac{1}{2}\delta))$	9
	F_3	I	$(u(t), u(t), u(t+\frac{1}{4}\delta), u(t+\frac{1}{4}\delta))$	10
	F_5	I	$(u(t), u(t+\frac{1}{4}\delta), u(t), u(t+\frac{1}{4}\delta))$	
$(\mathbf{Z}_3, \mathbf{1})$	V_1	I	$(v(t), u(t), u(t+\frac{1}{3}\delta), -u(t+\frac{2}{3}\delta))$	11
	V_3	I	$(u(t), v(t), -u(t+\frac{1}{3}\delta), u(t+\frac{2}{3}\delta))$	12
	V_5	I	$(u(t), -u(t+\frac{2}{3}\delta), v(t), u(t+\frac{1}{3}\delta))$	
	V_7	I	$(u(t), -u(t+\frac{1}{3}\delta), -u(t+\frac{2}{3}\delta), v(t))$	13
$(\mathbf{D}_4, \mathbf{Z}_4)$	F_1, A_2	F_1	$(u(t), u(t), u(t), u(t))$	14
	F_3, A_3	F_3	$(u(t), -u(t), u(t), -u(t))$	15
	F_5, A_1	F_5	$(u(t), u(t), -u(t), -u(t))$	

Table 4: Conjugacy classes of Hopf type states, and the associated patterns of muscle activation, where $\delta = \pm 1$, $u(t+\frac{1}{2}) = -u(t)$, $z(t+\frac{1}{2}) = -z(t)$, $v(t+\frac{1}{6}) = -v(t)$.

while $y_1(t) = v(t)$ is independent of these. However, the same phase shifts apply to y_1, so we must have $v(t) \equiv v(t+\frac{1}{3}\delta)$. Moreover, like every periodic state arising by Hopf bifurcation, v also satisfies $v(t+\frac{1}{2}) = -v(t)$. These observations lead to the condition $v(t+\frac{1}{6}) = -v(t)$ in the table.

Notice that for phase shifts other than $0, \frac{1}{2}$ the states come in pairs, with plus or minus the stated phase shift. These pairs are identical except for time-reversal. For a given imaginary eigenspace, either one of these states occurs or the other does, but not both. See [9, pp. 112–114]. (When $H/K \cong Z_m$ with $m = 5$ or $m \geq 7$ the same pair H/K can correspond to several distinct phase shifts, even taking the sign into account. For example, the $\mathbf{Z}_5$ case can have phase shift $\frac{2}{5}$ as well as $\frac{1}{5}$. However, these cases do not occur in the group $\mathbb{O}$.)

Table 4 lists (up to conjugacy) five small-amplitude periodic state types that can occur by

Hopf bifurcation supported by the standard 3-dimensional irreducible representation of $\mathbb{O}$, plus a sixth supported by the one-dimensional representation. We interpret these motions in terms of our caricature of the muscle groups. We will see that all six cases lead to repetitive motions that seem quite reasonable.

Conjugate states are determined by $\mathbb{O}/(N(H) \cap N(K))$

We briefly discuss the technical issue: states whose associated subgroups are conjugate.

Suppose that $x(t)$ is a periodic state with spatiotemporal symmetry group pair (H, K). Let $\gamma \in \Gamma$. Then $\gamma x(t)$ is a periodic state with spatiotemporal symmetry group pair (H', K'), where

$$H' = \gamma H \gamma^{-1} \quad \text{and} \quad K' = \gamma K \gamma^{-1}$$

So the symmetry group pairs are identical if and only if $\gamma \in N(H) \cap N(K)$ The number of conjugate periodic states with different spatiotemporal symmetries is

$$\frac{|\Gamma|}{|N(H) \cap N(K)|} \tag{5.3}$$

When we specialize to $\Gamma = \mathbb{O}$, the number of conjugates can be found by computing the normalizers of the appropriate subgroups. The normalizers are found in Table 2. In particular, $N(\mathbb{O}) \cap N(\mathbb{T}) = \mathbb{O}$, $N(\mathbf{S}_3) \cap N(\mathbf{Z}_3) = \mathbf{S}_3$, $N(\mathbf{D}_2^E) \cap N(\mathbf{Z}_2^E) = \mathbf{D}_2^E$, $N(\mathbf{Z}_4) = \mathbf{D}_4$, $N(\mathbf{Z}_3) = \mathbf{S}_3$, and $N(\mathbf{D}_4) \cap N(\mathbf{Z}_4) = \mathbf{D}_4$. It follows that the number of conjugacies of the six solution types are 1, 4, 6, 3, 4, 3, respectively, yielding 21 possibilities.

6 Head motions

The standard equivariant theory classifies solution types up to conjugacy by a symmetry element. However, conjugate states are important here: because, with one exception, the action of $\mathbb{O}$ on the muscle space network does not relate directly to motions of the head in physical space $\mathbf{R}^3$, and that exception is the bilateral (left-right) symmetry of the body, which is realized in our network by E_{45}. So, in general, conjugate symmetry groups can correspond to head motions that are substantially different. Counting conjugates, as we have in Table 4, leads to 21 motions to describe—28 if we include time-reversals for $\pm$ phase shifts. If we consider solution types up to time reversibility and bilateral symmetry, then there are 15 types to consider. The final column ('#') in Table 4 is a reference number which we will use to identify the various patterns of oscillation.

Description of motions listed in Table 4

To explain the derivation of Table 4, we take each conjugacy class in turn, and visualize the corresponding periodic state in the following manner. We assume, for simplicity, a two-dimensional description in which the head is modeled by a circle, as in Figure 7. The position of the neck is identified with the center of this circle. The orientation of the nose (under rotation about the neck axis) is specified by a vector based at the center of the circle with the appropriate orientation.

We decompose the head motion into two distinct components. The spatial motion of the head is obtained by summing the six vectors representing the muscle groups of the central dial. As time t varies through a cycle, the resultant vector describes a closed curve in the horizontal plane, schematically representing the motion of the center of the circle that represents the head position.

Rotations of the neck (caused by muscle groups LA, RA) are represented as rotations of the circle about its instantaneous center. These rotations are assumed to act independently of the translations of the circle. This assumption is invalid in the genuine three-dimensional motion, but it provides an adequate visualization of the small-amplitude motions, bearing in mind that Figure 7 is itself a caricature.

Next, we choose specific periodic functions u, z, v with the correct symmetry properties. For the figures drawn here we take

$$\begin{aligned} u(t) &= \sin(2\pi t) + 0.2\sin(10\pi t) \\ z(t) &= 0.75\sin(2\pi t) + 0.03\sin(10\pi t) \\ v(t) &= 0.3\sin(6\pi t) \end{aligned}$$

Then we use Table 4 to compute the six vectors of the central dial, and the rotation angle of the nose. We denote the center of the circle (head) as a function of time t by the curve $\mathcal{C}(t)$. For a periodic state $y(t) = (y_1(t), y_3(t), y_5(t), y_7(t))$ the closed curve $\mathcal{C}(t)$ has the form

$$\begin{aligned} \mathcal{C}_1(t) &= -2y_7(t) - y_3(t) - y_5(t) \\ \mathcal{C}_2(t) &= \sqrt{3}(y_3(t) - y_5(t)) \end{aligned} \tag{6.1}$$

The term $\sin(10\pi t)$ is included to remove some artificial regularities from the pictures, such as motions of the head in a perfect circle. The vector representing the orientation of the nose is drawn at times $\frac{n}{12}$ for $0 \leq n \leq 11$, as a vector based on the appropriate point of the curve $\mathcal{C}$, of fixed length.

This representation involves some arbitrary choices, but is adequate for our present needs. When interpreting the figures, note that $\mathcal{C}$ may reduce to a line segment (described twice) or even a single point. Also, the segments representing the nose may overlap each other, or overlap $\mathcal{C}$. These ambiguities can be resolved by creating a movie.

$(\mathbb{O}, \mathbb{T})$**:** Here the muscles of the central dial follow the pattern $y_3(t) = y_{\mathrm{LF}}(t) = -u(t)$, $y_5(t) = y_{\mathrm{LE}}(t) = -u(t)$, $y_7(t) = y_{\mathrm{LD}}(t) = u(t)$. From (6.1) we see that the curve $\mathcal{C}$ is a single point and the center of the head does not move. The nontrivial head motion comes from y_{LA} and y_{RA}, which swivel the head about its vertical axis. The overall invariance under $(-I, \frac{1}{2})$ implies that this swivel motion is the same as its left-right reflection, up to a half-period phase shift. This description corresponds exactly, under the assumptions of the model, to the usual 'shake the head' motion to indicate the word 'no'. The schematic visualization of this motion is shown in Figure 9. Here the nose vector oscillates from left to right to form the 'fan' shape illustrated.

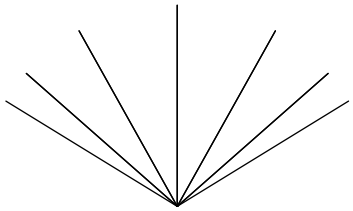

Figure 9: Motion for pattern 1 $(\mathbb{O}, \mathbb{T})$.

$(\mathbf{S}_3, \mathbf{Z}_3)$**:** If we take $H = \langle V_1, E_{15} \rangle$ and $K = \langle V_1 \rangle$, then this case turns out to be exactly like the previous one, except that the time series of the direct muscled motoneurons $u(t)$ is unequal to the time series of the central dial muscle motoneurons $z(t)$. Since the $z(t)$ motions cancel out, the motion again looks like 'no' and is reproduced as the first image in Figure 10. (Here angle brackets indicate the subgroup generated by their contents.)

The patterns for the other two conjugates of this motion can be deduced in a similar manner and are visualized in Figure 10. In pattern 3 the head is inclined alternately down to the left and up to the right, while the nose oscillates from side to side. In pattern 4, the head tilts alternately to left and right while the nose oscillates from side to side.

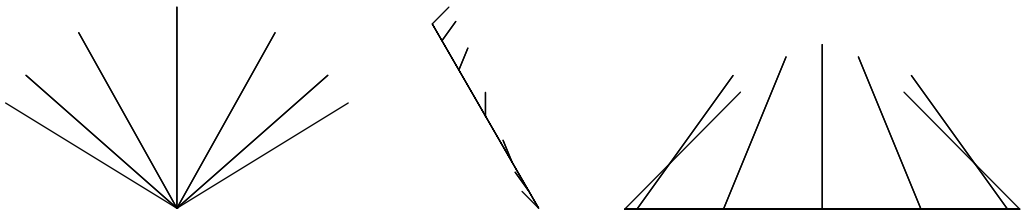

Figure 10: Motion for patterns 2-4 $(\mathbf{S}_3, \mathbf{Z}_3)$.

$(\mathbf{D}_2^E, \mathbf{Z}_2^E)$**:** First, we consider the conjugate state pattern 5 for which $K = \langle E_{16} \rangle$ and $H = \langle E_{16}, E_{15} \rangle$ and $y(t) = (u(t), u(t), 0, 0)$. The phase shift action of H/K implies that $u(t + \frac{1}{2}) =$

$-u(t)$. Now the muscle groups LD, RD, LE, RF are inactive; LA and LF are in phase with each other, and RA and RE are half a period out of phase with LA and LF. The head 'nods' down and to the left, then up and to the right, in roughly the direction of the muscle pair LF, RE, with a twist to the right as the head moves down, a twist to the left as it moves up. Another conjugate state has $K = \langle E_{14} \rangle$ and $H = \langle E_{14}, E_{13} \rangle$. This state is just the left/right image of the previous one.

Second, we consider pattern 6 where $K = \langle E_{45} \rangle$ and $H = \langle E_{45}, E_{35} \rangle$. Such a state has $y_{\mathrm{LA}} = y_{\mathrm{RA}} = y_{\mathrm{LD}} = y_{\mathrm{RD}} = 0$. The variables y_{LF} and y_{LE} are half a period out of phase, and the push-pull constraint implies that y_{RF} is in synchrony with y_{LF}, and similarly y_{RE} is in synchrony with y_{LE}. There is thus an overall left-right symmetry, and also a front-back symmetry when combined with a half period phase shift. This is precisely the pattern of movement observed when nodding the head (indicating 'yes'). Motions associated to patterns 7 and 8 are found similarly. Note that pattern 8 also corresponds to a standard head motion: one where the head rotates left as it tilts left and then it rotates right as it tilts right.

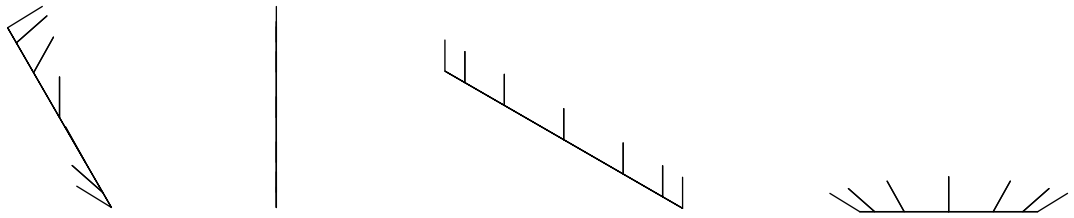

Figure 11: Motion for oscillation patterns 5-8 ($\mathbf{D}_2^E, \mathbf{Z}_2^E$).

($\mathbf{Z}_4, \mathbf{1}$): We take $H = \langle F_1 \rangle$. From Table 3, and noting that F_1 induces a phase shift of $\pm\frac{1}{4}$, we obtain the pattern listed in Table 4. (We also use the $(-I, \frac{1}{2})$ symmetry of all periodic states.) The motions are visualized in Figure 12.

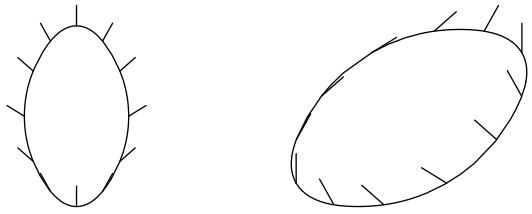

Figure 12: Motion for patterns 9-10 ($\mathbf{Z}_4, \mathbf{1}$).

In pattern 9, the head moves in an ellipse with long axis pointing towards the front. The nose oscillates from side to side, moving outwards at the front and inwards at the back. There are two conjugates in pattern 10 that are mirror images of each other. The motion is much as above, but the ellipse is oriented along a different axis.

$(\mathbf{Z}_3, \mathbf{1})$**:** Take $H = \langle V_1 \rangle$. This leads to the pattern stated in Table 4. Bearing in mind the $(-I, \frac{1}{2})$ symmetry, successive phases round the central dial differ by $\frac{1}{6}$. The head rotates in a 'circle' (strictly, a closed loop with hexagonal symmetry), combined with a swivel. Choice of plus or minus phase shifts produce clockwise or counterclockwise rotations. Conjugates here replace V_1 by V_3, V_5, V_7, noting that V_3 and V_5 are mirror images. The motions are visualized in Figure 13. In pattern 11 the head rotates in a rounded hexagonal curve, while the nose oscillates slightly. The other two patterns are more complicated and best described using the figure.

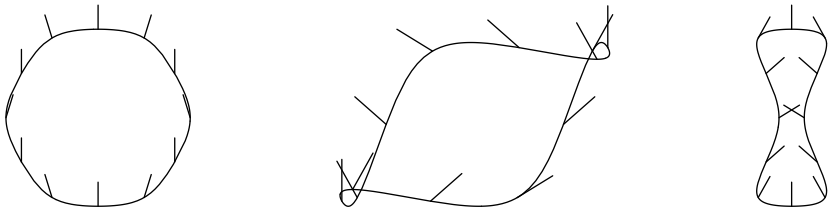

Figure 13: Motion for patterns 11-13 $(\mathbf{Z}_3, \mathbf{1})$.

$(\mathbf{D}_4, \mathbf{Z}_4)$**:** We choose $H = \langle F_3, A_3 \rangle$, $K = \langle F_3 \rangle$, and $y(t) = (u(t), -u(t), u(t), -u(t))$. The conjugates are as shown in Table 4. The motions are visualized in Figure 14. In each case the head moves in one of three planes (so $\mathcal{C}$ reduces to a line segment) while the nose oscillates from side to side. In pattern 14 the head moves left and right while the nose aims at a fixed central point.

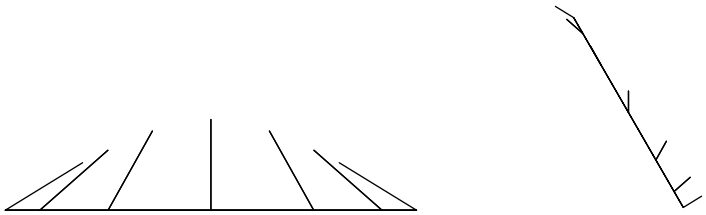

Figure 14: Motion for patterns 14-15 $(\mathbf{D}_4, \mathbf{Z}_4)$.

7 Conclusions

In Sections 2-4 we derived the octahedral symmetry of the canal-neck projection first discovered by McCollum and Boyle [12]. After conjecturing that the symmetry of the network of neck muscle motoneurons also has octahedral symmetry, we classified the spatiotemporal

symmetry types of small amplitude periodic solutions that can be obtained by Hopf bifurcaton. Finally, in Section 6, we used the caricature of muscle group actions develped in Section 2 to suggest the form that head motions might take.

On a cautionary note, the symmetries of neuronal networks need not reflect symmetries in the physical world. This happens in the network associated with orientation-tuned neurons in the primary visual cortex [2] and is also the case in the vestibular system. Thus, periodic solutions that are symmetrically related in the network need not be (obviously) related in physical space (actual head movements). We believe that the issue of network structure not being directly related to physical world structure will be important issue in many applications.

The next steps in the program we have described are to include in the model the (symmetry) structure of other projections in the vestibular system, for example the uvula-nodulus [7], to include the semicircular canals, and to make more direct contact with the biology. Two questions arise in this last step: Do the head motions we describe play some special role in the context of general periodic head motions (that is, do these motions appear frequently in animals), and can the classification of spatiotemporal symmetries of small amplitude motions near an upright head give a method for classifying types of head tremor? Our classification, which is based on the symmetries of a network that has been abstracted from the neurobiology of cat, provides a prediction for likely types of periodic head motions, much like the predictions that were implicit in our previous work on animal gaits [10, 11].

There may exist periodic states from other types of bifurcation, however, we classify the types undergo a Hopf bifurcation in this study.)

Appendix: Characters of the octahedral group

The most efficient way to decompose the space Y^- into irreducible representations of $\mathbb{O}$ or $\mathbb{O} \oplus \mathbf{Z}_2^c$ is to use character theory, see for example Curtis and Reiner [6]. Recall that for a given representation of a group Γ, the corresponding *character* χ is the function $\chi : \Gamma \to \mathbf{C}$ for which $\chi(\gamma)$ is the trace of the matrix that represents the action of $\gamma \in \Gamma$. We assume familiarity with character theory.

First, observe that any representation (space) U for $\mathbb{O}$ naturally determines two distinct representations U^+, U^- of $\mathbb{O} \oplus \mathbf{Z}_2^c$ with the same underlying vector space. In both, the elements of $\mathbb{O}$ have the same action as they do on U. The action of $-I$ on U^+ is by the identity, whereas that on U^- is by minus the identity. If U is irreducible for the action of $\mathbb{O}$ then the $U^\pm$ are irreducible for the action of $\mathbb{O} \oplus \mathbf{Z}_2^c$.

It is easy to prove that every irreducible for $\mathbb{O} \oplus \mathbf{Z}_2^c$ arises in this manner, as follows. Every irreducible representation of $\mathbb{O}$ is absolutely irreducible, so by Schur's Lemma the only commuting linear maps are scalar multiples of the identity. Since $-I$ commutes with

$\mathbb{O}$ and $(-I)^2 = I$, it follows that $-I$ must act as plus or minus the identity. The rest is straightforward.

Therefore we can read off the irreducible representations of $\mathbb{O} \oplus \mathbf{Z}_2^c$ from those of $\mathbb{O}$. It is well known (see for example Curtis and Reiner [6] 331–333) that $\mathbb{O}$ has five distinct irreducible representations: two of dimension 1, one of dimension 2, and two of dimension 3.

We can describe the irreducible representations of $\mathbb{O}$ as follows:

- ρ_0: dimension 1; trivial action.
- ρ_1: dimension 1; $\mathbb{T}$ acts trivially, $\mathbb{O} \setminus \mathbb{T}$ acts by -1.
- ρ_2: dimension 2; kernel is the Klein four-group $\mathbf{D}_2^A$, modulo which $\mathbb{O}$ acts in the standard representation of $\mathbf{D}_3$ on $\mathbf{R}^2$.
- ρ_3: dimension 3; standard action of $\mathbb{O}$ as isometries of $\mathbf{R}^3$ preserving the cube.
- ρ_4: dimension 3; nonstandard action on $\mathbf{R}^3$ in which $\mathbb{T}$ acts as rotations but $\mathbb{O} \setminus \mathbb{T}$ acts as rotations composed with minus the identity. In fact, $\rho_4 = \rho_1 \otimes \rho_3$. This representation is also isomorphic to the standard action of $\mathbf{S}_4$ on the subspace of $\mathbf{R}^4$ consisting of points whose coordinates sum to 0.

The conjugacy classes of $\mathbb{O}$ are also five in number. In the notation of Table 3 they are:

$$\{I\} \quad \{A_j\} \quad \{V_j\} \quad \{F_j\} \quad \{E_j\}$$

The character table for $\mathbb{O}$ is shown in Table 5, and is derived in Curtis and Reiner [6, pp. 332–333]. It is easy to compute the character χ of the $\mathbb{O}$-action described in Table 3, which is shown in Table 5 in the same format. In particular, we see that $\chi = \rho_1 + \rho_3$. Since characters determine representations uniquely, and direct sums of representations correspond to sums of characters, we see that Y^- decomposes into two irreducible components, the non-trivial one-dimensional representation and the standard three-dimensional representation. This is what we claimed in Section 4.

Acknowledgments

We thank Gin McCollum, Patrick Roberts, Douglas Hanes, David Romano, and Paul Matthews for helpful discussions. This work was supported in part by NSF Grant DMS-0244529. The work of IS was supported in part by a grant from EPSRC. The authors thank the Newton Institute, University of Cambridge, and the Department of Mathematics, University of Toronto for their hospitality.

	$\{I\}$	$\{A_j\}$	$\{V_j\}$	$\{F_j\}$	$\{E_j\}$
ρ_0	1	1	1	1	1
ρ_1	1	1	1	-1	-1
ρ_2	2	2	-1	0	0
ρ_3	3	-1	0	1	-1
ρ_4	3	-1	0	-1	1
χ	4	0	1	0	-2

Table 5: Character table for representations of $\mathbb{O}$.

References

[1] P. Ashwin and O. Podvigina. Hopf bifurcation with cubic symmetry and instability of ABC flow, *Proc. R. Soc. Lond. A* **459** (2003) 1801–1827.

[2] P.C. Bressloff, J.D. Cowan, M. Golubitsky, P.J. Thomas, and M.C. Wiener. Geometric visual hallucinations, Euclidean symmetry, and the functional architecture of striate cortex. *Phil. Trans. Royal Soc. London B* **356** (2001) 299–330.

[3] P.L. Buono and M. Golubitsky. Models of central pattern generators for quadruped locomotion: I. Primary gaits, *J. Math. Biol.* **42** No. 4 (2001) 291–326.

[4] J.J. Collins and I. Stewart. Hexapodal gaits and coupled nonlinear oscillator models, *Biol. Cybern.* **68** (1993) 287–298.

[5] J.J. Collins and I. Stewart. Coupled nonlinear oscillators and the symmetries of animal gaits, *J. Nonlin. Sci.* **3** (1993) 349–392.

[6] C.W. Curtis and I. Reiner. *Representation Theory of Finite Groups and Associative Algebras*, Wiley Interscience, New York 1962.

[7] I.Z. Foster, D.A. Hanes, N.H. Barmack, and G. McCollum. Spatial Symmetries in Vestibular Projections to the Uvula-Nodulus. Preprint.

[8] M. Golubitsky and I.N. Stewart. Hopf bifurcation in the presence of symmetry, *Arch. Rational Mech. Anal.* **87** No. 2 (1985) 107–165.

[9] M. Golubitsky and I. Stewart. *The Symmetry Perspective*, *Progress in Mathematics* **200**. Birkhäuser Verlag, Basel 2002.

[10] M. Golubitsky, I. Stewart, P.-L. Buono, and J.J. Collins. A modular network for legged locomotion, *Physica D* **115** (1998) 56–72.

[11] M. Golubitsky, I. Stewart, P.-L. Buono, and J.J. Collins. Symmetry in locomotor central pattern generators and animal gaits, *Nature* **401** (1999) 693–695.

[12] G. McCollum and R. Boyle. Rotations in a vertebrate setting: evaluation of the symmetry group of the disynaptic canal-neck projection. *Biol. Cybern.* **90** (2004) 203–217.

[13] P.M. Neumann, G.A. Stoy, and E.C. Thompson. *Groups and Geometry*, Oxford University Press, Oxford 1994.

[14] Y. Shinoda, Y. Sugiuchi, T. Futami, N. Ando, and T. Kawasaki. Input patterns and pathways from six semicircular canals to motoneurons of neck muscles I: The multifidus muscle group, *J. Neurophysiology* **72** (1994) 2691–2702.

[15] Y. Shinoda, Y. Sugiuchi, T. Futami, N. Ando, and J. Yagi. Input patterns and pathways from six semicircular canals to motoneurons of neck muscles: II, The longissimus and semispinalis muscle groups, *J. Neurophysiology* **72** (1997) 2691–2702.

[16] Y. Shinoda, Y. Sugiuchi, T. Futami, S. Kakei, Y. Izawa, and J. Na. Four convergent patterns of input from the six semicircular canals to motoneurons of different neck muscles in the upper cervical cord, *Annals New York Acad. Sci.* **781** (1996) 264–275.

[17] T. Vilis. The physiology of the senses, Lecture 10: Balance, www.med.uwo.ca/physiology/courses/sensesweb

[18] V.J. Wilson and M. Maeda. Connections between semicircular canals and neck motoneurons in the cat, *J. Neurophysiology* **37** (1974) 346–357.